Sports Technology
Publication details, including instructions for authors and subscription information:
http://www.tandfonline.com/loi/rtec20

Speed measurements in wheelchair sports - theory and application

Franz Konstantin Fuss [a]
[a] School of Aerospace, Mechanical and Manufacturing Engineering, Royal Melbourne Institute of Technology (RMIT) University, Melbourne, Australia
Version of record first published: 21 Dec 2012.

To cite this article: Franz Konstantin Fuss (2012): Speed measurements in wheelchair sports - theory and application, Sports Technology, 5:1-2, 29-42

To link to this article: http://dx.doi.org/10.1080/19346182.2012.754895

Sports Technology, February–May 2012; 5(1–2): 29–42

Routledge
Taylor & Francis Group

RESEARCH REVIEW

Speed measurements in wheelchair sports – theory and application

FRANZ KONSTANTIN FUSS

School of Aerospace, Mechanical and Manufacturing Engineering, Royal Melbourne Institute of Technology (RMIT) University, Melbourne, Australia

(*Received 25 November 2012; accepted 28 November 2012*)

Abstract
Speed measurements should be the standard in high-performance wheelchair sports, specifically for track racing. The required technology (triaxial gyroscopes and data logger) is nowadays no longer an obstacle, as smartphones are ubiquitous. Based on gyroscope raw data, in particular data obtained from smartphones attached to the wheels, the following performance parameters can be calculated: the true wheel speed, turning speed and sense, turning radius and linear wheelchair speed. The true wheel speed is obtained from the kinematics of a planetary bevel gear. Based on speed profiles, weak points, such as discontinuous acceleration and sudden drops in velocity, can be identified. Further performance parameters are calculated from speed profiles, such as peak acceleration, consistency of push frequency, push and recovery time and ratio of push to recovery time. Furthermore, speed profiles provide the basis for simulating winning times, if the speed profile is optimised (changing weak points to the ideal speed profile), or wheelchair parameters are changed, such as drag coefficient, rolling friction coefficient or mass.

Keywords: *wheelchair, speed, velocity measurements, gyroscope, smart phone, iPhone, acceleration, push frequency, bevel gear, track racing*

Introduction

In sports disciplines, the performance of which is governed by maximal acceleration and speed as well as best winning times, velocity measurements should be the standard for performance analysis. In most cases, the available technology constrains the full potential of advanced measurements of performance parameters. For example, the first optical computer mice were invented in 1980, the first commercially successful optical mouse was available in 1999 and the first commercial ski speedometer was launched in 2008 (Kirby, 2009), which is based on the principle of optical mouse technology.

Therefore, it is not surprising how little is known about practical wheelchair speed measurements and their application for performance analysis in training and competition, in spite of the availability of relatively accurate, low cost and, even most importantly, ubiquitous sensor systems.

In many cases, it is not just the (unavailable) technology which prevents performance analysis, but rather the data analysis, the extraction of performance parameters, and the decisions and interventions based on the processed data. In other words, these issues are related to the question: 'what can we do with the raw data?' or 'can we use speed measurements for anything other than measuring the speed?'.

The aim of this paper is to provide an overview of

- simple yet sufficiently accurate wheelchair speed measurements;
- speed data processing and analysis;
- performance parameters of athletes and wheelchairs; and
- decision making and training intervention.

The paper is based on the author's experience obtained from working with, and providing technological support to, elite wheelchair athletes (most of

Correspondence: Franz Konstantin Fuss, School of Aerospace, Mechanical and Manufacturing Engineering, Royal Melbourne Institute of Technology (RMIT) University, Melbourne, Australia. E-mail: franz.fuss@rmit.edu.au

ISSN 1934-6182 print/ISSN 1934-6190 online
http://dx.doi.org/10.1080/19346182.2012.754895

which competed at the Paralympic Games level) over the last 7 years.

Methods of wheelchair speed measurement

This section reviews briefly available methods for speed measurement and their practical application for competition and training on court and track.

(1) Kinematic measurement systems. Camera-based systems are relatively expensive and insufficiently accurate. For automated analysis, wheelchairs are equipped with markers. Several cameras are required for covering even short distances such as 100 m. Most kinematic systems are not suited for outdoor use. Data extraction and analysis can be very labour intensive. Chow and Chae (2007) used two S-VHS camcorders (60 fields/s) for covering the first and second half of a 100-m race and for obtaining speed profiles.

(2) Magnetic sensors detect the number of revolutions per unit time from a spoke-mounted magnet. As the speed changes within a single revolution, which is inherent to pushing a wheelchair, magnetic sensors are too inaccurate.

(3) Velocimeters for continuous measurement of the (true) speed of a wheel:
These devices bridge the frame and the wheel with additional joints or pairs (higher and/or lower pairs), with one pair acting as a sensor. Velocimeters can be in direct contact with the wheel or hub (rolling or sliding) or use contactless measurement techniques.
   (a) direct rolling contact:
      – vintage bicycle speedometers with gears or cogwheels;
      – encoders, e.g. optical encoders (Moss, Fowler, & Tolfrey, 2003; Figure 1(a));
      – electric motors/generators with linear relationship of EMF (electro-motive force, voltage generating) and speed (Fuss & Ow, 2008a, 2008b; Fuss 2009; Figure 1(b),(c)).
      These devices are mounted on the frame and are in contact with the wheel, directly with the hub (Figure 1(c)) or a disc mounted on the spokes (Figure 1(a),(b)). They are driven through a small wheel (Figure 1) or pinion.
   (b) contactless or frictionless sliding:
      – optical devices with CCD (e.g. optical computer mouse; c.f. Kirby, 2009, for linear speed measurements).
      These devices can be mounted on the frame and are in sliding contact with a disc mounted on the spokes.

(4) Velocimeters for continuous measurement of the speed of a wheel (with true speed and turning speed confounded):
Microelectromechanical systems (MEMSs) gyroscopes are nowadays the cheapest and most accurate solution for measurements of angular velocity. These gyroscopes are mounted on the wheel but not connected to the wheelchair frame. Therefore, they do not measure the angular velocity with respect to the frame but rather with respect to the environment. The analysis of gyroscope data and the calculation of true speed are described in detail in the next section. This is insofar of importance, as gyroscopes are nowadays ubiquitous, as most smartphones have inbuilt gyros and provide a convenient measurement platform with sensors, data logger, recording app and software for data download.

Theory and application of speed measurements with MEMS gyros

Speed measurements with gyroscopes

As wheels are in rolling contact with the ground, the wheelchair system can be modelled as a set of planetary bevel gears with a single carrier (Figure 2). For purely linear movements (with infinite turning radius), the bevel gears reduce to a rack and pinion mechanism (inclined in cambered wheels). In Figure 2, the planets correspond to the wheels which are in rolling contact with the ground link, comprised of the fixed bevel sun and bevel ring gear.

Figure 1. Instrumentation of wheelchairs with speed sensors: (a) optical encoder (Moss, Fowler, & Tolfrey, 2003; © Elsevier, reproduced with kind permission); (b) and (c) electric motor (Fuss 2009; © Springer, reproduced with kind permission).

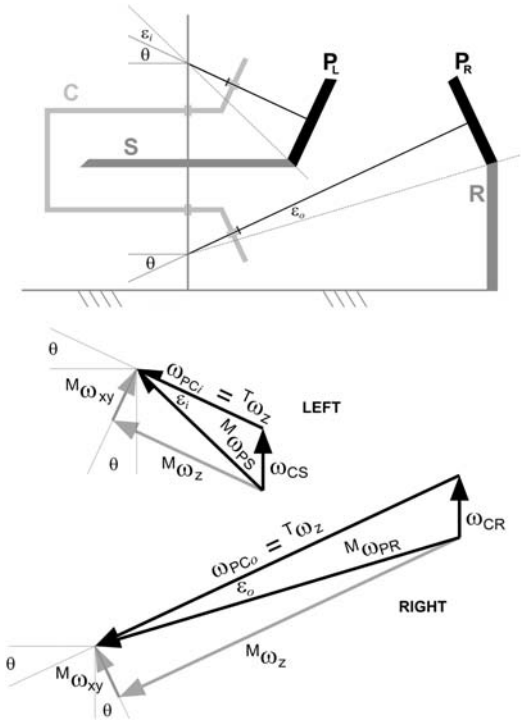

Figure 2. Schematic of a planetary bevel gear representing a rolling and turning wheelchair and vector diagrams of angular velocities; S, bevel sun; R, bevel ring gear (only right half shown); C, carrier; P_L and P_R, left (inner) and right (outer) planets (wheels of a wheelchair in rear view, rolling forward and turning left); θ, camber angle; ε_i and ε_o, inner and outer pitch cone angles; ω_{CS} and ω_{CR}, carrier speed about sun and ring (true turning speed of the frame); ω_{PCi} and ω_{PCo}, inner and outer planet speed about the carrier; ${}^T\omega_z$, true z-speed (true wheel speed); ${}^M\omega_{PS}$ and ${}^M\omega_{PR}$, planet speed about sun and ring (measured resultant speed); ${}^M\omega_z$, measured speed about z-axis of the wheel; ${}^M\omega_{xy}$, measured speed about axes perpendicular to z (resultant of ω_x and ω_y located in the plane of the wheel).

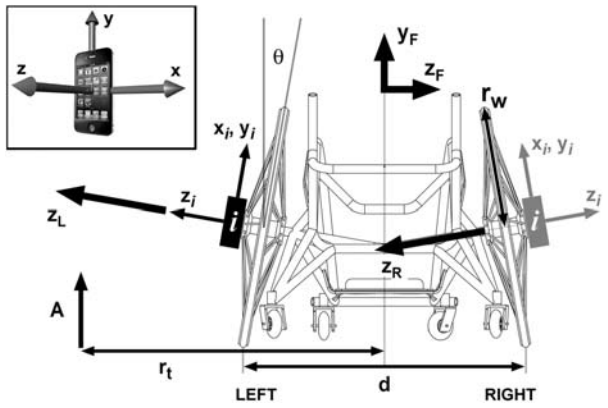

Figure 3. Geometrical parameters and coordinate systems (rear view of a rugby wheelchair); θ, camber angle; r_w, wheel radius; d, the track width; A, axis about which the frame turns; 'i', iPhone mounted on wheel; zi, z-axis of iPhone; xi and yi, position of xy resultant parallel to the plane of the wheel; z_L and z_R, z-axis of the left and right wheels; y_F and z_F, y- and z-axes of wheelchair frame; insert top left corner: iPhone coordinate system. Rugby wheelchair design and figure courtesy by Clara Cristina Usma-Alvarez.

The outer planet meshes with the ring. The carriers of the planets are integral and from a single carrier, corresponding to the frame of the wheelchair. The carrier rotates about the sun/ring shaft, which corresponds to the turning axis of the frame.

A triaxial gyroscope, connected to and located in a plane parallel to the wheel, measures the angular velocity of the wheel with respect to the ground:

- ${}^M\omega_z$ = measured speed about z-axis of the wheel (Figure 3); and
- ${}^M\omega_{xy}$ = measured speed about axes perpendicular to the z-axis (resultant of ω_x and ω_y, located in the plane of the wheel).

The measured ω_z, however, does not correspond to the true speed of the wheel if the frame is turning:

- ${}^T\omega_z$ = true z-speed = angular velocity of wheel with respect to the frame.

In order to relate these velocities (${}^M\omega_z$, ${}^T\omega_z$ and ${}^M\omega_{xy}$) to the planetary bevel gear, the following subscripts are used subsequently:

- P = bevel planet = wheel;
- S = bevel sun = ground;
- R = bevel ring gear = ground;
- C = carrier = wheelchair frame.

The velocities of the bevel gear are as follows:

- ω_{CS} (ω_{CR}) = carrier speed about the sun (ring) = true turning speed of the frame;
- ω_{PC} = planet speed about the carrier = ${}^T\omega_z$ = true speed about the z-axis = true wheel speed;
- ω_{PS} (ω_{PR}) = planet speed about the sun (ring) = ${}^M\omega_{PS}$ (${}^M\omega_{PR}$) = measured resultant speed.

Subsequently, only S is used as subscript, for both inner and outer wheels.

True wheel speed

The vector diagrams of the different angular velocities are shown in Figure 2.

In a left wheel turning left, ${}^M\omega_z > {}^T\omega_z$ (Figure 2), and therefore

$$\tan\theta = \frac{{}^M\omega_z - {}^T\omega_{PC}}{{}^M\omega_{xy}}. \quad (1)$$

The true speed of the wheel results from

$${}^T\omega_{PC} = {}^M\omega_z - {}^M\omega_{xy}\tan\theta. \quad (2)$$

In a right wheel turning left, ${}^{M}\omega_z < {}^{T}\omega_z$ (Figure 2), and therefore

$$\tan\theta = \frac{{}^{T}\omega_{\mathrm{PC}} - {}^{M}\omega_z}{{}^{M}\omega_{xy}}. \tag{3}$$

The true speed of the wheel results from

$${}^{T}\omega_{\mathrm{PC}} = {}^{M}\omega_z + {}^{M}\omega_{xy}\tan\theta. \tag{4}$$

When using two triaxial gyros for measuring the speed of left and right wheel, the sensors must be positioned such that one sensor axis is aligned to the hub axis, which has to point leftward (the angular velocity vector of a forward rolling wheel points to the left; Figure 3). When using two smartphones, their z-axes point in different directions, in order to have access to the touch screen for activating the app. In this case, the components ω_{xyz} of the angular velocities of the right wheel and smart phone are multiplied by -1.

The frame coordinate system (x – forward, y – upward, z – to the right) is oriented such that the camber angle θ is positive on left wheel (x-axis pointing forward) and negative on right wheel. When considering the sign of the camber angle, Equations (1) and (2) remain unchanged, whereas in Equations (3) and (4), the tangent term becomes negative such that Equation (4) changes and becomes identical to Equation (2). This solves the left/right wheel problem. However, the turning problem is not solved yet as Equations (1)–(4) refer to left turns only, although Equations (1) and (2) also apply to a *right wheel turning right* and Equations (3) and (4) to a *left wheel turning right*. In order to address the direction of rolling at the same time as the sense of turning, the turning direction has to be defined by the direction of the movement of the wheelchair front:

- when rolling forward and turning left, the wheelchair front turns left and the sense of turning is positive;
- when rolling forward and turning right, the wheelchair front turns right and the sense of turning is negative;
- when rolling backward and turning left, the wheelchair front turns right and the sense of turning is negative;
- when rolling backward and turning right, the wheelchair front turns left and the sense of turning is positive.

This solves the turning and rolling issue, as, in general, the wheelchair front turns *left* (positive turning sense) if $\omega_{z\,\mathrm{RIGHT}} > \omega_{z\,\mathrm{LEFT}}$. When rolling forward, the right wheel is the outer one and has a higher velocity. When rolling backward with a positive sense of turning, the left wheel is the outer one and thus has a higher but negative velocity such that still $\omega_{z\,\mathrm{RIGHT}} > \omega_{z\,\mathrm{LEFT}}$ applies. In order to accommodate for a negative turning sense, the tangent term of Equation (2) has to be multiplied by the sign function of $(\omega_{z\,\mathrm{RIGHT}} - \omega_{z\,\mathrm{LEFT}})$, which delivers a positive sign if the turning sense is positive:

$${}^{T}\omega_{\mathrm{PC}} = {}^{M}\omega_z - {}^{M}\omega_{xy}\tan\theta\,\mathrm{sgn}\,(\omega_{z\mathrm{RIGHT}} - \omega_{z\mathrm{LEFT}}). \tag{5}$$

In their Equation (6), Pansiot, Zhang, Lo, & Yang (2011) distinguished between the right and left wheel (with the multiplier δ_{RL}, which is $+1$ in the right and -1 in the left wheel). As shown in Equation (5), the true wheel speed does not depend on the side where the wheel is located (as this is taken care of by the sign of the camber angle) but rather on the sense of turning.

Turning speed and sense

Considering a positive camber angle θ of the left wheel, and a positive sense of ${}^{M}\omega_z$ and ${}^{T}\omega_{\mathrm{PC}}$ when rolling forward, the vector diagrams of Figure 2 result in

$$\omega_{\mathrm{CS}} = \frac{{}^{M}\omega_z - {}^{T}\omega_{\mathrm{PC}}}{\sin\theta}, \tag{6}$$

which delivers correct sign of the sense of turning.

Turning radius

As inner and outer wheels have a common carrier,

$$\frac{r_{\mathrm{t}} - (d/2)}{\omega_{\mathrm{PCi}}} = \frac{r_{\mathrm{t}} + (d/2)}{\omega_{\mathrm{PCo}}}, \tag{7}$$

where r_{t} is the turning radius, d is the track width and subscripts i and o stand for inner and outer wheel, respectively.

Solving for r_{t},

$$r_{\mathrm{t}} = \frac{d}{2}\left(\frac{\omega_{\mathrm{PCo}} + \omega_{\mathrm{PCi}}}{\omega_{\mathrm{PCo}} - \omega_{\mathrm{PCi}}}\right). \tag{8}$$

As $\omega_{\mathrm{PCo}} > \omega_{\mathrm{PCi}}$ when turning, replacing the angular velocity of the inner and the outer wheel by the one of the left and the right wheel

$$r_{\mathrm{t}} = \frac{d}{2}\left(\frac{\omega_{z\mathrm{RIGHT}} + \omega_{z\mathrm{LEFT}}}{\omega_{z\mathrm{RIGHT}} - \omega_{z\mathrm{LEFT}}}\right), \tag{9}$$

delivers positive r_{t} for positive turns. If $\omega_{z\,\mathrm{RIGHT}} = \omega_{z\,\mathrm{LEFT}}$, then $r_{\mathrm{t}} = \pm\infty$, as the wheelchair is progressing linearly. If $\omega_{z\,\mathrm{RIGHT}} = -\omega_{z\,\mathrm{LEFT}}$, then $r_{\mathrm{t}} = 0$, as the wheelchair turns on the spot. As the turning

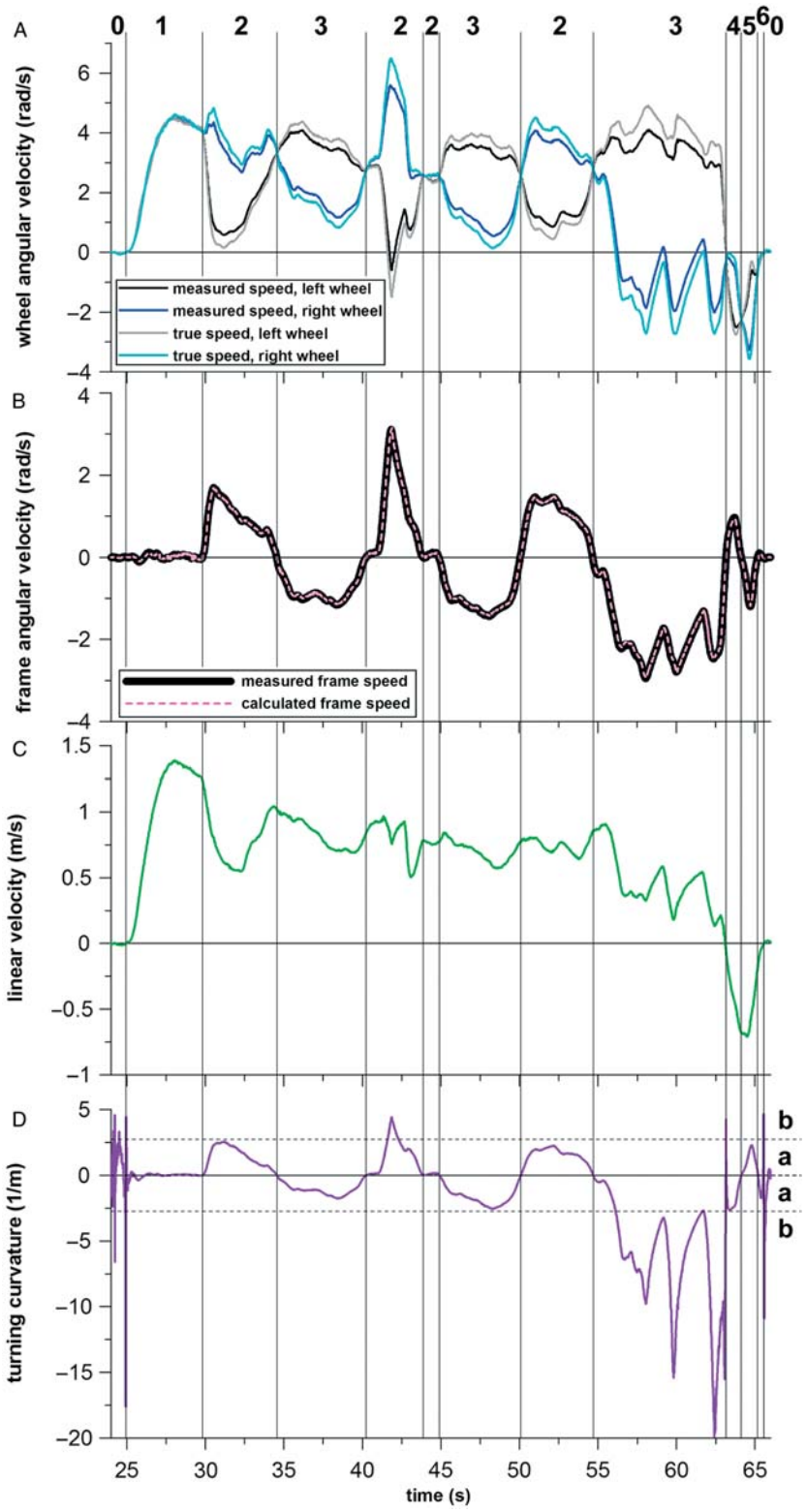

Figure 4. Angular (wheels: A; frame: B) and linear (C) velocities, and turning curvature (D; reciprocal of turning radius) against time (experiment with rugby wheelchair; camber angle: 17°; track width: 726 mm; and wheel radius: 305 mm); 0 = no movement; 1 = linear movement forward; 2 = rolling forward, front of chair turns left; 3 = rolling forward, front of chair turns right; 4 = rolling backward, front of chair turns left; 5 = rolling backward, front of chair turns right; 6 = linear movement backward; *a* = centre of rotation between wheels (turning radius < half of track width); *b* = centre of rotation outside track width; A: positive angular velocity if wheels turning forward (right view of wheelchair); B: positive angular velocity if front of chair turns left; C: positive linear velocity if chair rolls forward; D: positive turning curvature if front of chair turns left.

radius is infinite when progressing linearly, it is advisable to plot the turning curvature rather than the turning radius (Figure 4(D)). The turning curvature is the reciprocal value of the turning radius.

Linear velocity

From common gearing principles, the linear velocity v at rolling contact (contact of pitch radii) is

$$v = \omega_{CS}\, r_t = \omega_{PC}\, r_w, \tag{10}$$

where r_w is the wheel radius. The linear velocity v_c of the wheelchair's centre point (intersection of symmetry and wheel contact lines) in turning and purely linear movements equals

$$v_c = r_w\left(\frac{\omega_{zRIGHT} + \omega_{zLEFT}}{2}\right). \tag{11}$$

If the wheelchair turns on the spot (about its centre), then $v_c = 0$.

It is advisable to verify whether the linear velocity v_c calculated matches the actual wheelchair speed. This can be achieved by properly calibrating the gyroscopes and applying a correction factor. Alternatively, a wheelchair equipped with two triaxial gyroscopes is moved over a distance of exactly 100 m (at variable speeds including maximally possible speed), and the v_c is integrated with time. The time integral, i.e. the distance, should be 100 m. If this is not the case, then v_c is multiplied by a constant (assuming that the error is not speed dependent) in order to obtain a distance of exactly 100 m.

Procedure for measuring wheel speed with gyroscopes and smartphones

The data recording frequency should not be smaller than 100 Hz. In wheelchair racing, even for linear speeds approaching 10 m/s, 100 Hz is still sufficient. The input data required for calculating the parameters listed below are the raw speed data ω_{xyz} of both wheels and the geometrical data of the wheelchair (Figure 3), i.e. camber angle θ (positive on left wheel, negative on right wheel), wheel radius r_w and the track width d. The procedure of calculation is as follows:

- change the sign of ω_{xyz} of right wheel when using smartphones;
- calculate the true wheel speed from Equation (5);
- calculate the turning speed from Equation (6);
- calculate the turning radius from Equation (9); and
- calculate the linear wheelchair speed from Equation (11).

An experiment was carried out with three 4G iPhones, one mounted on each wheel and one located on the frame of a rugby wheelchair ($\theta = 17°$, $r_w = 305$ mm, $d = 726$ mm). The latter served for measuring the turning speed and comparing it to the one calculated from the two iPhones mounted on the wheels. The graphs are shown in Figure 4. The calculated and measured angular velocities of the frame (ω_{CS}) are in good agreement. The percentage difference between the calculated and measured (3rd iPhone) turning speed equals 1.84 times the calculated turning speed (average from first and second iPhone) to the power of -0.715. If the turning speed is 3, 1 or 0.1 rad/s, then the error of the unfiltered data is 0.9%, 2% or 10%, respectively.

Speed measurements for optimisation purposes

The term 'optimisation' refers to aerodynamics, friction and mass. Speed measurements provide information on the aerodynamics of athlete, apparel (e.g. helmet and garments) and chair; on the rolling friction between the chair (e.g. tyres and casters) and surfaces (e.g. wooden court surface and granulated rubber track surface) and on how the mass of the chair influences the winning time. Aerodynamic assessment of athlete (different body positions during recovery and push phases; different apparel) and chair (aerodynamic modifications) is particularly important if paralympic sports organisations, coaches and athletes do not have access to wind tunnels.

Coast-down experiments

Coast-down experiments provide direct information on aerodynamic drag and rolling friction of an athlete–wheelchair system or a wheelchair without athlete. The chair is sped up by an assistant to a reasonable speed and then left to coast down until still stand. During this exercise, the speed of the chair is recorded. The chair (with or without athlete) is slowed down due to aerodynamic drag and rolling resistance. The guidelines for performing coast-down experiments are:

- avoid experiments in windy conditions (or indoor draft);
- perform experiments in two opposite directions in order to account for uneven or slightly slanted surfaces as well as minimal or unpredictable air movement;
- perform aerodynamic experiments always with the athlete, preferably in at least two different positions (with minimal and maximal frontal area);
- if rolling resistance experiments (different wheels and tyres) are carried out without athletes, then

the wheelchair must be loaded with additional weights in order to compensate for the athlete's body weight.

When coasting down, three forces are in equilibrium (static position of the athlete provided):

- the inertial force, F_I, of the athlete–wheelchair system, pointing forward and produced by the deceleration of the system: $F_I = a\,m = m\,dv/dt$, the product of acceleration a (the rate change of the velocity v with time t) and mass m;
- the drag force, F_D, pointing backward and produced by air resistance: $F_D = 0.5\,\rho A d\,v^2$, where ρ is the air density, Ad is the drag area (the product of drag coefficient and frontal area) and v is the velocity of the system; and
- the rolling friction force, F_R, pointing backward and produced by rolling resistance: $F_R = \mu\,m\,g$, where μ is the coefficient of rolling friction and $m\,g$ is the weight (product of mass m and gravitational acceleration g; note that lift effects can alter the weight).

From the force equilibrium,

$$m\frac{dv}{dt} + c_1 v^2 + c_2 = 0, \tag{12}$$

where the constants $c_1 = 0.5\,\rho A d + k\,m\,g$ and $c_2 = \mu\,m\,g$. The constant k is the non-linear, velocity-dependent term of the rolling friction. This means aerodynamic drag and non-linear rolling resistance are confounded in c_1 and cannot be separated. However, $k \ll 0.5\,\rho A d$ in racing wheelchairs (Fuss 2009) and therefore k has an insignificant effect on aerodynamic drag. Nevertheless, aerodynamic drag and rolling resistance should be assessed from separate coast-down experiments: for aerodynamic experiments, the mass and the rolling resistance should be kept constant (same tyres, inflation pressure and surface); for rolling resistance experiments, the body position of the athlete, the frontal area of chair and athlete and the air temperature should be the same for all experiments.

Solving the non-linear differential Equation (12) for v yields

$$v_t = \sqrt{\frac{c_2}{c_1}}\tan\left[\tan^{-1}\left(v_0\sqrt{\frac{c_1}{c_2}}\right) - t\frac{\sqrt{c_1 c_2}}{m}\right], \tag{13}$$

where v_0 is the initial velocity. Fitting coast-down speed data with Equation (13) delivers the coefficients c_1 and c_2 (Figure 5). As $c_1 \ll c_2$, the coast-down method is more sensitive to changes in rolling resistance (and mass) than to changes in aerodynamic drag.

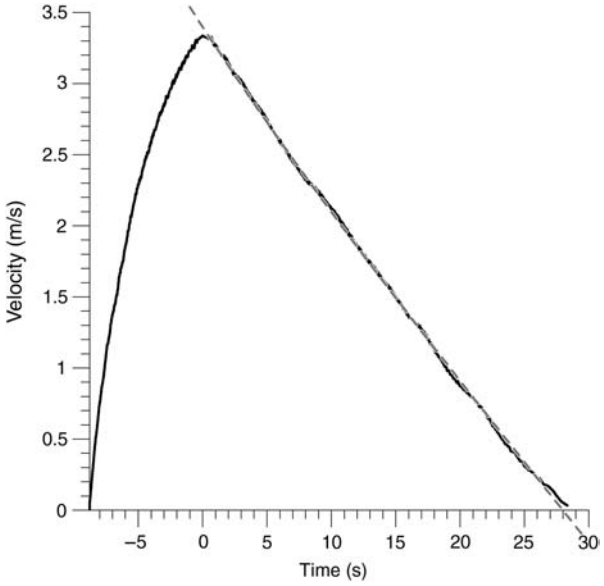

Figure 5. Coast-down experiment. Initial velocity at beginning deceleration: 3.4 m/s. solid curve: velocity against time; dashed curve: data fitted with Equation (13); from Fuss (2009); © Springer, reproduced with kind permission.

Modelling of the winning time

Aerodynamics, rolling friction and mass directly influence the winning time in wheelchair track racing. The effect of these parameters can be easily simulated based on speed profiles of, for example, a 100-m race. Based on a specific speed profile, i.e. velocity against time over, for example, 100 m, two different races are simulated with exactly the same input energy but different mass, drag coefficient or rolling friction coefficient (Fuss 2009). The athlete's energy expenditure is calculated from the kinetic energy (from the speed profile) plus the energy losses from aerodynamic drag and rolling resistance, and a continuous rather than a cyclic energy supply is simulated. As both races are simulated over the same distance, the problem reduces to equalling the input forces (or applied forces, F_A) which are the distance derivative of the input energy:

$$-F_A = F_{I1} + F_{D1} + F_{R1}, \tag{14}$$

$$-F_A = F_{I2} + F_{D2} + F_{R2}, \tag{15}$$

$$F_{I1} + F_{D1} + F_{R1} = F_{I2} + F_{D2} + F_{R2}. \tag{16}$$

Equation (16) is expanded to

$$M_1\frac{d^2x}{dt_1^2} + (C_{D1} + m_1 g\,k_1)\frac{dx^2}{dt_1^2} + m_1\mu_1 g = M_2\frac{d^2x}{dt_2^2} + (C_{D2} + m_2 g\,k_2)\frac{dx^2}{dt_2^2} + m_2\mu_2 g, \tag{17}$$

where C_D is the lumped drag coefficient ($0.5\,\rho Ad$) and M is the equivalent mass:

$$M = m + \sum_{i=1}^{3} \frac{I_i}{r_i^2}, \tag{18}$$

and r_i is the radius of wheel i and I_i is the moment of inertia of wheel i.

Solving Equation (17) for dt_2 yields

$$dt_2 = \sqrt{\frac{dt_1^2[M_2 d^2x + (C_{D2} + m_2 g\, k_2)dx^2]}{M_1 d^2x + (C_{D1} + m_1 g\, k_1)dx^2 + dt_1^2 g(\mu_1 m_1 - \mu_2 m_2)}}. \tag{19}$$

Numerical integration of Equation (19) delivers the solution of t_2 as a function of aerodynamic, rolling friction and mass parameters, as well as secondarily of t_1 and distance x. t_1 and t_2 at $x = 100$ m, for example, correspond to the expected winning times.

Out of the three parameters, mass is the most important one for reducing the winning time, and aerodynamic drag is the least important one (Fuss 2009). Reduction of the aerodynamic drag by 10% improves the winning time only by 1–2%.

Equation (17) is a useful tool for assessing the effect of wheelchair modifications, even before performing speed measurements for quantifying the effect of these modifications on the wining time. For example, improvement of the lift of a wheelchair reduces its weight and therefore the rolling resistance. This is implemented in Equation (20), where mass, coefficient of drag and rolling resistance remain unchanged. The wheelchair is equipped with a massless airfoil, which not only generates the lift force but also contributes to drag.

$$M\frac{d^2x}{dt_1^2} + C_D\frac{dx^2}{dt_1^2} + mg\mu = M\frac{d^2x}{dt_2^2} + C_D\frac{dx^2}{dt_2^2} + C_{D1}\frac{dx^2}{dt_2^2} + mg\mu - \mu\left(\frac{L}{D}\right)C_{D1}\frac{dx^2}{dt_2^2}. \tag{20}$$

C_{D1} is the lumped drag coefficient of the airfoil (which adds to the drag coefficient C_D of the athlete–wheelchair system). L/D is the lift to drag ratio of the airfoil. L/D multiplied by C_{D1} yields the lumped lift coefficient of the airfoil, which in turn, multiplied by v^2 delivers the lift force, multiplied by μ results in the amount by which the rolling friction force is reduced. Instead of assessing by how much the airfoil improves the winning time, the condition that does *not* change the winning time is explored. This is due to the fact that the lift force advantageously reduces the winning time, but the additional drag force of the airfoil has an adverse effect. If the winning times of left and right sides of Equation (20) are identical, then $dt_1 = dt_2$.

$$M\frac{d^2x}{dt_1^2} + C_D\frac{dx^2}{dt_1^2} + mg\mu = M\frac{d^2x}{dt_1^2} + C_D\frac{dx^2}{dt_1^2} + C_{D1}\frac{dx^2}{dt_1^2} + mg\mu - \mu\left(\frac{L}{D}\right)C_{D1}\frac{dx^2}{dt_1^2}. \tag{21}$$

After simplifying, $\mu(L/D) = 1$, or

$$\frac{L}{D} = \frac{1}{\mu}. \tag{22}$$

In order to improve the winning time, $L/D > 1/\mu$. Considering a rolling resistance coefficient μ of 0.011 (racing wheelchair plus athlete on rubber track; Fuss 2009) or 0.005 (unloaded rugby wheelchair on wooden court surface; Chua, Fuss, & Subic, 2011), L/D must be >91 or >200, respectively. These high lift-to-drag ratios are unfeasible and require extremely high aspect ratios, which cannot be implemented in racing wheelchairs.

Speed measurements for analysis and improvement of performance

In this section, performance parameters of wheelchair racing are derived and explained, and a case study for decision making is presented. The performance parameters comprise speed profiles, stroke frequency, and push and recovery time and ratio.

Speed profiles

Figure 6 shows the speed profiles of 100-m training races of four different athletes (two male T53, and one female and male T52; three of them qualified at least once for Paralympic Games; two of them participated at least once in Paralympic Games and one of them is a multiple gold medallist). The speed profiles of athletes A, C and D (Figure 6) were recorded with a generator (electric motor), and the one of athlete B was recorded with two 4G iPhones.

The speed profiles give immediate feedback on weak points, such as cusps (continuous and increasing velocity but discontinuous acceleration; Figure 6(C)) or decreasing velocity (sudden decrease in Figure 6(D) or gradual decrease due to fatigue). If the speed profiles are plotted against time, then the weak points and the problems causing them can be identified on video footage. In order to compare profiles with different winning times, the velocity is plotted against time or distance. The distance (in metres) is obtained from (numerically) integrating the velocity over time. As the cyclic changes of the velocity (increasing when pushing, decreasing during recovery) make it difficult to compare profiles of

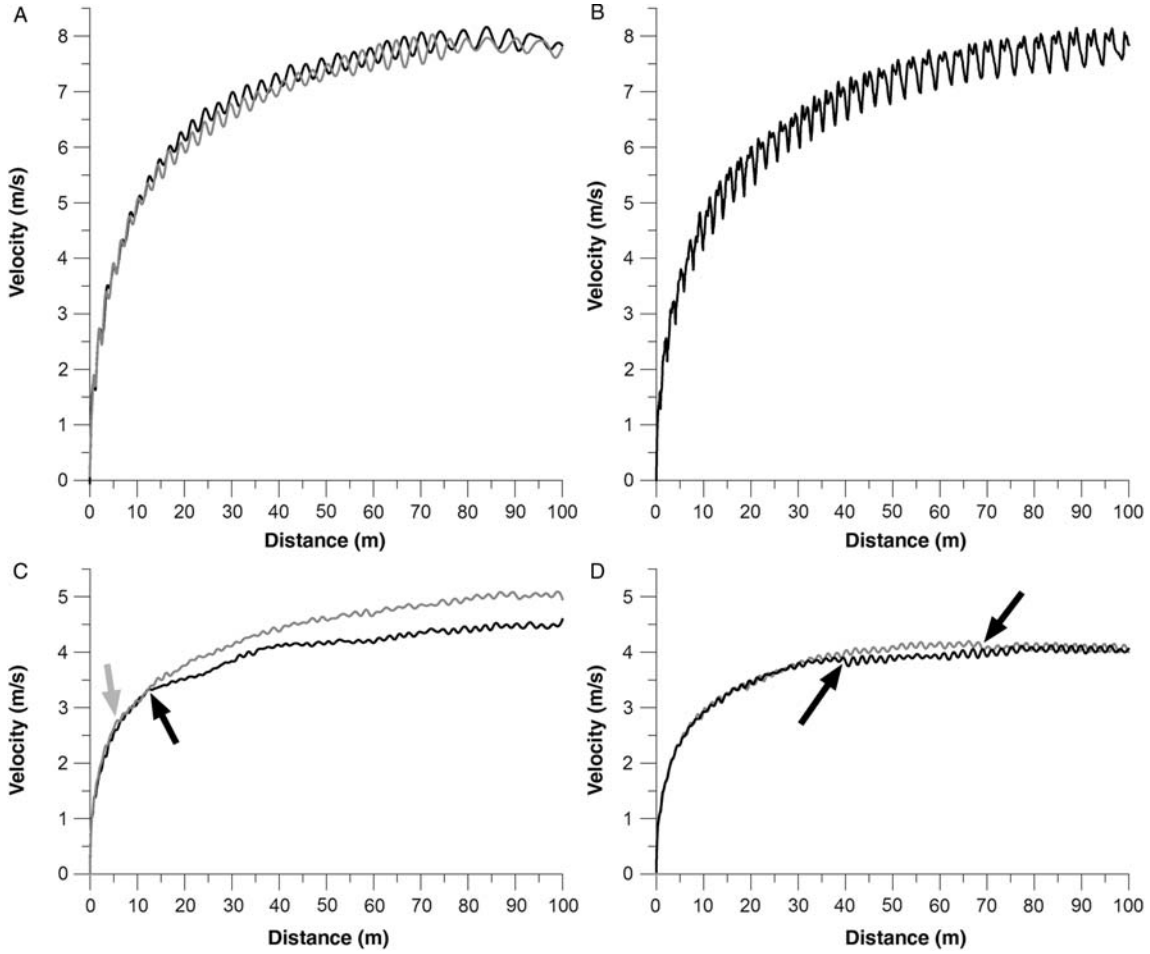

Figure 6. Velocity profiles against distance of male T53 (A and B) and male (C) and female (D) T52 athletes; black arrow in C: cusp (discontinuous acceleration); grey arrow in C: not immediately apparent cusp; arrows in D: slight drop in velocity.

similar shape, a reciprocal function

$$v = \frac{\mathrm{d}x}{\mathrm{d}t} = \frac{A}{B} - \frac{A}{t^C + B} \tag{23}$$

can be fitted in the speed profiles (Fuss 2009). Profiles fitted with Equation (23) are shown in Figure 7(a). The coefficients A, B and C are determined numerically by fitting the original velocity profile with Matlab (MathWorks, Natick, MA, USA). A is a general multiplier, which depends on the maximal velocity and thus on the winning time. The fit curves allow comparing different speed profiles in terms of the magnitude of the velocity (coefficient A) and by how much the actual speed profile deviates from the fit curve. The latter parameter identifies the consistency of the speed profile, and where/when and by how much the athlete under- or over-performs (Figure 7(a)). It is advisable to fit only ideal speed profiles without apparent weak points, or to remove segments of underperformance before fitting. Athlete C, for example, significantly underperforms between 3.5 and 14 s (grey arrows in Figure 7(a)) compared to the ideal fit curve. This is not immediately apparent without fitting the speed profile; however, a slight cusp of the speed profile at 3.5 s into the race indicates a discontinuity of the acceleration (grey arrow in Figure 6(C)). Comparing athletes A and B shows that athlete A generates a higher acceleration at the beginning of the race but a smaller acceleration at the end compared to athlete B. This result can be verified by differentiating Equation (23) which provides the acceleration of the fitted speed profile (Figure 7(b)).

$$a = \frac{\mathrm{d}^2x}{\mathrm{d}t^2} = \frac{AC\,t^{C-1}}{\left(t^C + B\right)^2} \tag{24}$$

Equation (24) models the acceleration with a zero value at the beginning of the race

$$\lim_{t \to 0} AC \frac{t^{C-1}}{\left(t^C + B\right)^2} = 0, \tag{25}$$

followed by an acceleration peak, and finally the acceleration approaches zero asymptotically

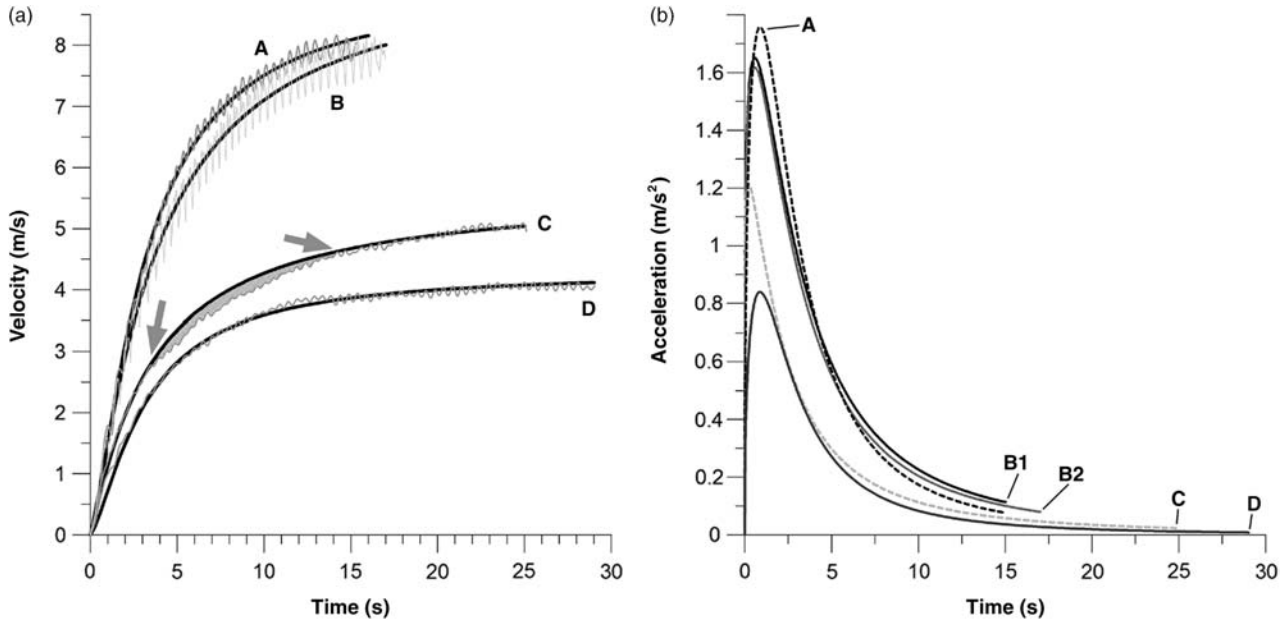

Figure 7. Velocity data (a) fitted with Equation (23) and acceleration (b) of the fitted velocity data; grey arrows: segment where athlete C underperforms compared to the ideal fit curve; the left grey arrow corresponds to the grey arrow in Figure 6(C).

(applying l'Hôpital's rule in Equation (26)).

$$\lim_{t\to\infty} AC\frac{t^{C-1}}{\left(t^C+B\right)^2} = \lim_{t\to\infty}\frac{A(C-1)}{2}\frac{1}{t\left(t^C+B\right)} = 0 \quad (26)$$

Figure 7(b) verifies the different acceleration behaviour of athletes A and B, already mentioned above. The higher the acceleration at the beginning of the race, the faster the athlete reaches maximal speed and the better is the winning time. Therefore, the acceleration peak in Figure 7(b) is the most important performance parameter. The two curves of athlete B (B1 and B2 in Figure 7(b)) correspond to first and third 100 m race. The acceleration in the third race is slightly smaller than that in the first one, which accounts for muscle fatigue.

Push frequency

A further important parameter is the push frequency, how consistent it is and how it changes with distance and time (Figure 8). The push frequency is not necessarily constant after the main acceleration phase during which the frequency increases. Athletes A and B increase the push frequency initially up to 2.5 Hz, followed by a decrease down to 1.5–2 Hz (Figure 8(A),(B)). Athletes C and D keep the push frequency constant at 2 Hz. It is, however, imperative that the push frequency remains as consistent as possible. The consistency can be measured with the residual standard deviation when fitting a polynomial (e.g. of the fifth order) to the push frequency data shown in Figure 8. Athlete B has the least residual standard deviation of 0.09 Hz, followed by athlete D with 0.16 Hz, athlete A with 0.2 Hz and athlete C with 0.4 Hz. That 'wheelchair athletes prefer to maintain the same stroking rhythm when stroking with maximum effort' (Chow & Chae, 2007) does not apply to the two T53 athletes (Figure 8).

Push and recovery periods

Push and recovery periods behave differently at different stages of a race (Figure 9). At the beginning, the push period can be close to 1 s in the first push and then decreases to 0.25 s. The recovery period is initially <0.25 s and finally approaches 0.25 s. In athlete A, both push and recovery periods increase to 0.35–0.4 s at the end of the 100 m race. These results, namely equal push and recovery periods at the end of a 100-m race as well as highly different push and recovery periods at the beginning, stand in sharp contrast to the results of Chow and Chae (2007). They report the opposite, specifically equal push and recovery periods at the beginning (0.274 and 0.271 s, respectively) and highly different push and recovery periods in the middle and at the end (0.116–0.117 and 0.398–0.43 s, respectively).

The ratio of push to recovery period is shown in Figure 10. The ratio in the first stroke is between 7 and 16 in the four athletes and then drops to 2 at the

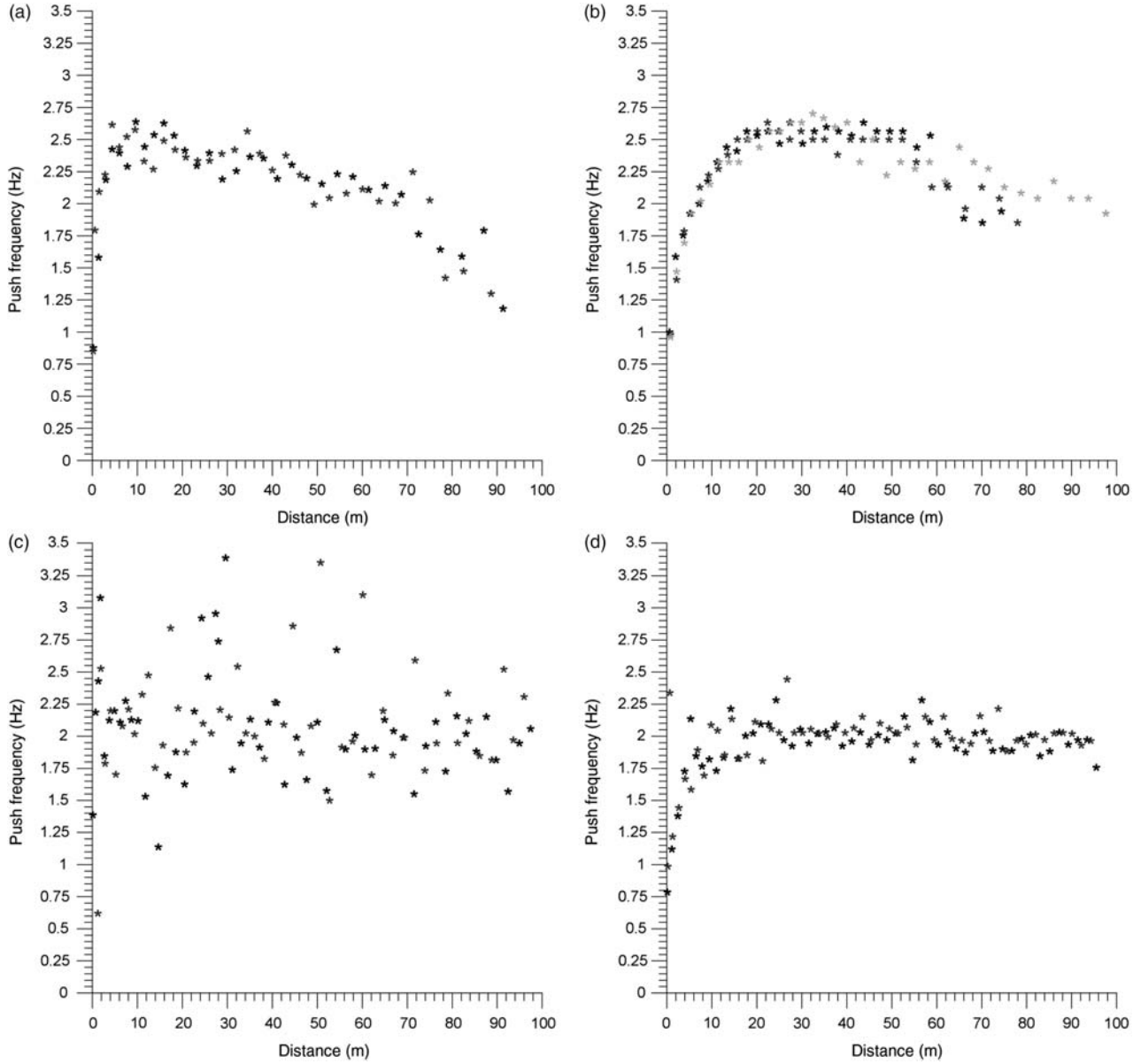

Figure 8. Push frequency against distance (shades of grey represent different track races).

end of the acceleration phase [1 on average in the acceleration phase according to Chow and Chae (2007)]. The ratio asymptotes to 1 after 40–70 m in all four athletes [0.27–0.29 according to Chow and Chae (2007)].

Case report

The stroke pattern of athlete B, magnified in Figure 11, exhibits discontinuous acceleration with a small deceleration period after the first push acceleration. At that point, energy is taken out of the system and the reason of the energy loss has to be explored.

There are three possibilities of cyclic energy loss:

- arm accelerations/decelerations in the middle of the push phase cause a temporary deceleration of the wheelchair;
- the movements of arm and hand cannot keep up with the wheel speed and generate a slight braking effect;
- the hand is temporarily taken off the pushrim and the energy is taken out by aerodynamic drag and rolling resistance.

The first possibility was excluded by testing the athlete on a wheelchair ergometer, which delivered

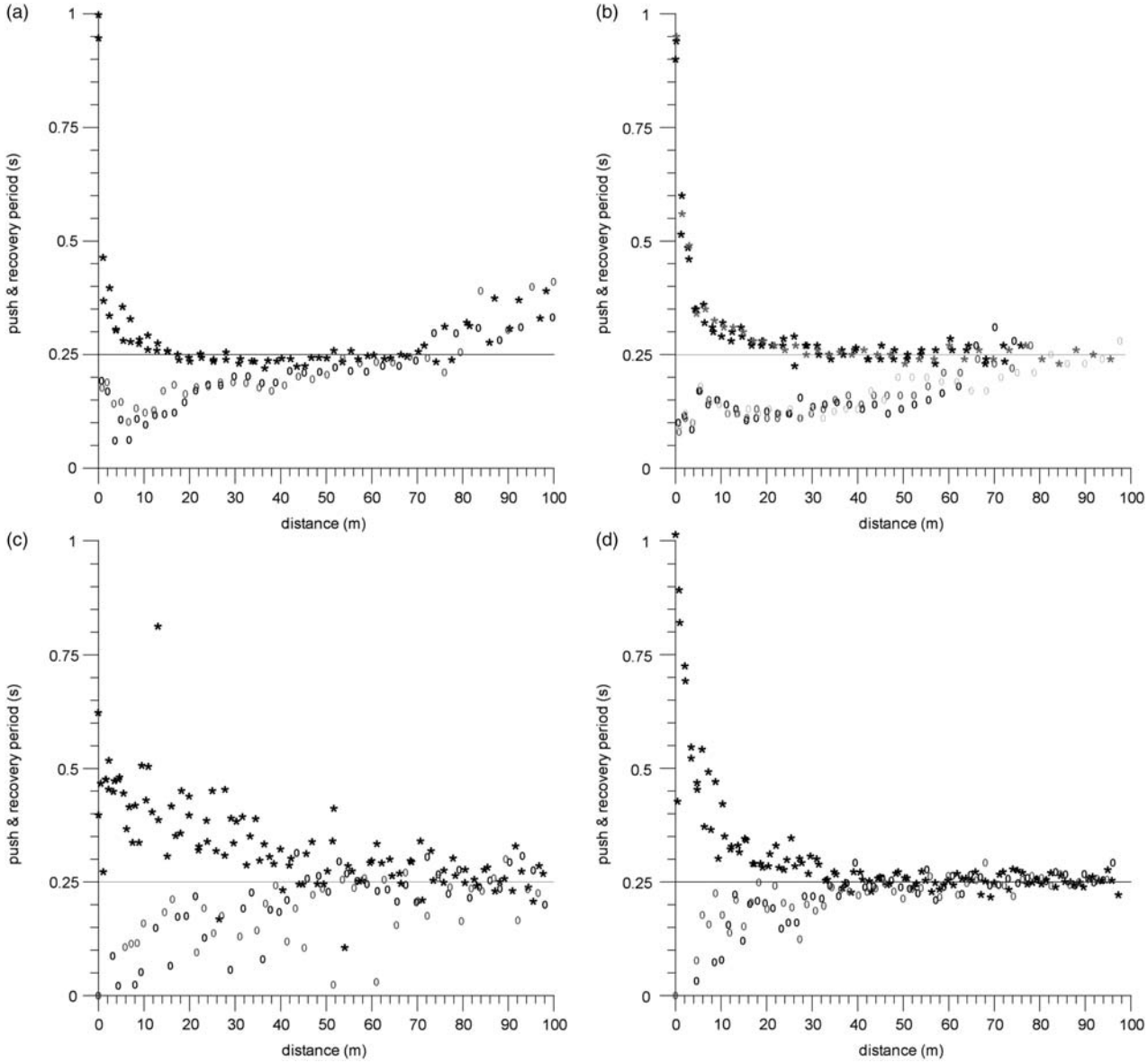

Figure 9. Push (*) and recovery (0) periods against distance (shades of grey represent different track races).

exactly the same speed profile. The third possibility was excluded with video analysis. The question whether any training intervention is required in order to reduce the energy loss can be answered by simulating the race without any energy loss by including area '1' (Figure 11) in the profile and secondarily by simulating a parabolic speed profile of the stroke (areas '1' and '2'; Figure 11). The gain in winning time when removing the trough and adopting a flat stroke peak is 0.04 s in 100 m, and when generating a parabolic stroke peak amounts to 0.08 s. These gains are relatively small when considering that reducing the mass of the wheelchair by merely 1 kg would have improved the winning time of athlete B by 0.15–0.2 s.

Conclusions

This research review provides a straightforward procedure for calculating the true wheel speed, turning speed and sense, turning radius and linear wheelchair speed when using gyroscopes, and in particular, smartphones with inbuilt gyroscopes. Based on speed profiles, weak points can be identified and further performance parameters calculated, such as peak acceleration, consistency of push frequency, push and recovery time and ratio of push to recovery

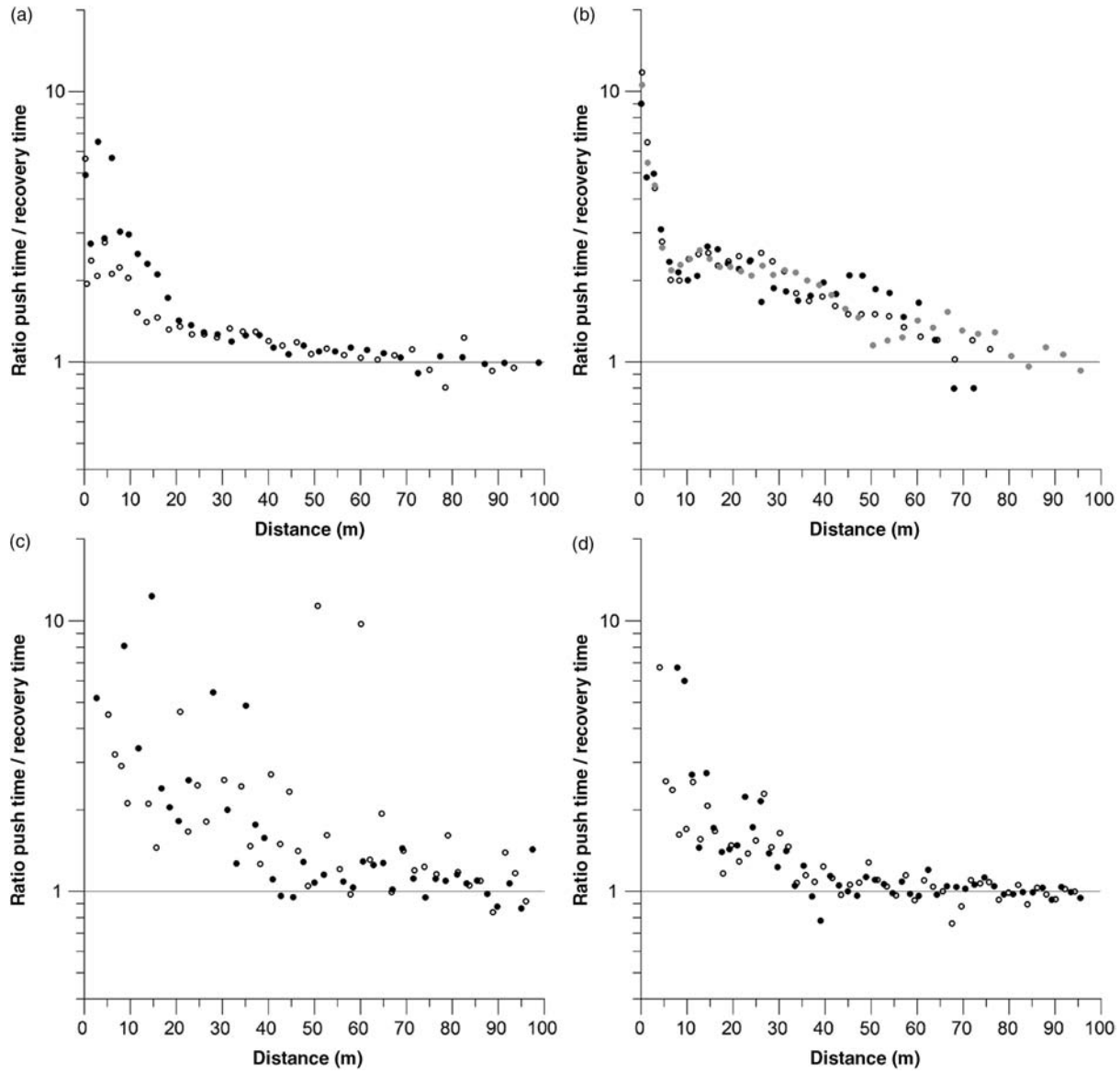

Figure 10. Ratio of push to recovery period against distance (open and filled black and grey circles represent different track races).

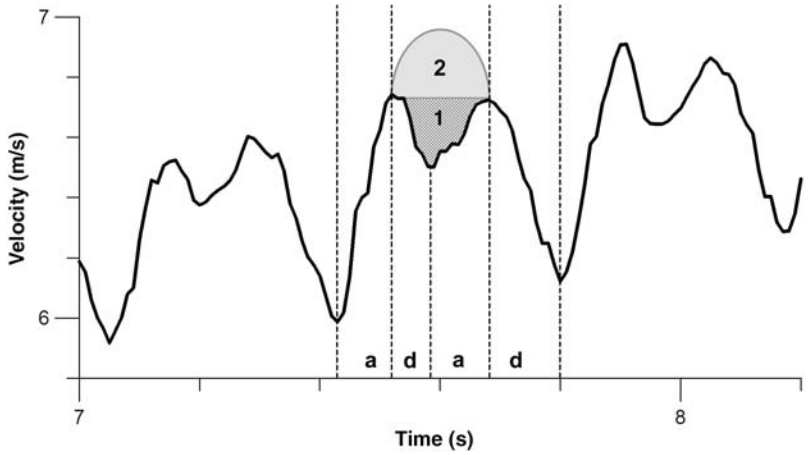

Figure 11. Magnified speed profile against time; *a*, acceleration phase; *d*, deceleration; 1 and 2, alternative (simulated) profiles for estimating the winning time.

time. Furthermore, speed profiles provide the basis for simulating winning times, if the speed profile is optimised, or wheelchair parameters are changed, such as drag coefficient, rolling friction coefficient or mass.

References

Chow, J. W., & Chae, W.-S. (2007). Kinematic analysis of the 100-m wheelchair race. *Journal of Biomechanics*, *40*, 2564–2568.

Chua, J. J. C., Fuss, F. K., & Subic, A. (2011). Non-linear rolling friction of a tyre-caster system: Analysis of a rugby wheelchair. *Proceedings of the Institution of Mechanical Engineers, Part C, Journal of Mechanical Engineering Science*, *225*, 1015–1020.

Fuss, F. K., & Ow, Z. E. J. (2008a). Performance Diagnostics with instrumented racing wheelchairs: Comparison of athletes of class T52 and T53. ISBS 2008, XXVI International Symposium on Biomechanics in Sports, July 14–18, 2008, Seoul, Korea (pp. 320–323).

Fuss, F. K., & Ow, Z. E. J. (2008b). Identification of Performance indicators in wheelchair racing., CDSTC2008 Classifying Disability and Sports Technology Conference, Nov. 20–22, Singapore.

Fuss, F. K. (2009). Influence of mass on the speed of wheelchair racing. *Sports Engineering*, *12*, 41–53.

Kirby, R. (2009). Development of a real-time performance measurement and feedback system for alpine skiers. *Sports Technology*, *2*, 43–52.

Moss, A. D., Fowler, N. E., & Tolfrey, V. L. (2003). A telemetry-based velocometer to measure wheelchair velocity. *Journal of Biomechanics*, *36*, 253–257.

Pansiot, J., Zhang, Z., Lo, B., & Yang, G. Z. (2011). WISDOM: Wheelchair inertial sensors for displacement and orientation monitoring. *Measurement Science and Technology*, *22*, 105801(9pp).